Acta Cryst. (1994). D**50**, 826–832

Refined Crystal Structure of *Acinetobacter glutaminasificans* Glutaminase–Asparaginase

BY JACEK LUBKOWSKI, ALEXANDER WLODAWER, DOMINIQUE HOUSSET* AND IRENE T. WEBER†

Macromolecular Structure Laboratory, NCI-Frederick Cancer Research and Development Center, ABL-Basic Research Program, Frederick, MD 21702-1201, *USA*

HERMAN L. AMMON AND KENAN C. MURPHY‡

Department of Chemistry and Biochemistry, University of Maryland, College Park, MD 20742, *USA*

AND AMY L. SWAIN

Macromolecular Structure Laboratory, NCI-Frederick Cancer Research and Development Center, ABL-Basic Research Program, Frederick, MD 21702-1201, *USA*

(*Received* 6 *October* 1993; *accepted* 29 *March* 1994)

Abstract

The crystal structure of glutaminase–asparaginase from *Acinetobacter glutaminasificans* has been reinterpreted and refined to an R factor of 0.171 at 2.9 Å resolution, using the same X-ray diffraction data that were used to build a preliminary model of this enzyme [Ammon, Weber, Wlodawer, Harrison, Gilliland, Murphy, Sjölin & Roberts (1988). *J. Biol. Chem.* **263**, 150–156]. The current model, which does not include solvent, is based in part on the related structure of *Escherichia coli* asparaginase and is significantly different from the structure of the enzyme from *A. glutaminasificans* described previously. The reason for the discrepancies has been traced to insufficient phasing power of the original heavy-atom derivative data, which could not be compensated for fully by electron-density modification techniques. The corrected structure of *A. glutaminasificans* glutaminase–asparaginase is presented and compared with the preliminary model and with the structure of *E. coli* asparaginase.

Introduction

Amidohydrolases catalyze the hydrolysis of asparagine and/or glutamine to aspartic acid/glutamic acid, respectively. The glutaminase–asparaginase isolated from *Acinetobacter glutaminasificans* (AGA; Roberts, Holcenberg & Dolowy, 1970) belongs to the family of amidohydrolases that consist of chemically identical subunits related by 222 symmetry (Epp, Steigemann, Formanek & Huber, 1971; Roberts, Holcenberg & Dolowy, 1972; Ammon *et al.*, 1983). These tetrameric enzymes have four active sites, each located between different lobes of adjacent subunits (Swain, Jaskólski, Housset, Rao & Wlodawer, 1993; Miller, Rao, Wlodawer & Gribskov, 1993) (Fig. 1). Tetrameric bacterial amidohydrolases from different sources have molecular weights of approximately 140 000, share about 40% sequence similarity, have highly conserved regions around the active site and have similar affinity for their substrates ($K_m \simeq 10^{-5}$–10^{-6} M; Wade, 1980).

Because the tetrameric amidohydrolases have antitumor properties, some of these enzymes are used clinically for treatment of leukemias and lymphomas that are sensitive to asparagine depletion. Although AGA posseses antitumor activity (Roberts *et al.*, 1970), it is not the enzyme of choice for therapeutic purposes because it has broad specificity for its substrates (Holcenberg & Roberts, 1977). On the other hand, the amidohydrolases from *Escherichia coli* (EcA) and *Erwinia chrysanthemi* (ErA), which are more specific for asparagine, are used clinically for the treatment of acute lymphoblastic leukemia (Roberts, Schmid, Old & Stockert, 1976).

For several years, our crystallographic investigations focused on an orthorhombic form of AGA because its asymmetric unit contains only one monomer and the 222 symmetry of the tetramer is expressed crystallographically (Wlodawer, Roberts & Holcenberg, 1977). Intensity data for the native crystals extending to 2.9 Å and for three heavy-atom

* Current address: Institut de Biologie Structurale, Laboratoire de Cristallographie et Cristallogénèse des Protéines, 41 avenue des Martyrs, 38027 Grenoble CEDEX 1, France.

† Current address: Department of Pharmacology, Jefferson Cancer Institute, Thomas Jefferson University, 233 South 10th Street, Philadelphia, PA 19107, USA.

‡ The work described in this manuscript is taken in part from the PhD dissertation of K. C. Murphy, University of Maryland, 1983.

Table 1. *Relative occupancies and fractional coordinates for the three heavy-atom derivatives of AGA*

Values in parentheses were calculated using AGA88 phases. The occupancies have been rescaled with respect to that of the first site of the *p*-chloromercuribenzoate derivative, assumed to be 1.00. The mean figure of merit is 0.78 (0.75) for the resolution range 14.0 (20.0)–4.0 Å.

Derivative	Resolution (Å)	Reflections	Occupancy	*x*	*y*	*z*	R_{Cullis} (%)
Sodium mersalyl	5.3	1454	0.88	0.3347	0.3613	0.3936	
			(1.46)	(0.3368)	(0.3673)	(0.3929)	
			0.42	0.1749	0.7899	0.3014	46
			(0.97)	(0.1833)	(0.7850)	(0.3000)	(55)
			0.39	0.1254	0.2145	0.4288	
			0.39	0.0037	0.3194	0.2214	
			(0.48)	(0.0043)	(0.3239)	(0.2304)	
Platinum ethylenediamine dichloride	4.0	3068	0.64	0.0008	0.3221	0.2329	
			(1.01)	(0.0088)	(0.3231)	(0.2370)	
			0.63	0.3367	0.3521	0.3888	45
			(0.64)	(0.3393)	(0.3539)	(0.3891)	(42)
			0.26	0.3015	0.5260	0.1174	
			(0.28)	(0.2982)	(0.5278)	(0.1232)	
p-Chloromercuribenzoate	4.7	1689	1.00	0.3321	0.3646	0.3927	
			(1.00)	(0.3327)	(0.3657)	(0.3974)	
			0.27	0.1149	0.8928	0.0901	46
			(0.23)	(0.1112)	(0.8975)	(0.0930)	(46)
			0.23	0.0214	0.0099	0.3455	

derivatives extending to 4.5–5.3 Å resolution were collected and, as a result, AGA became the first amidohydrolase for which an atomic model was obtained (Ammon *et al.*, 1988). That model, built before the AGA sequence (Tanaka *et al.*, 1988) was known, will be referred to as AGA88. Because of the relatively low resolution of the X-ray data, particularly for the heavy-atom derivatives, AGA88 contained errors that could not be corrected without additional data. Unfortunately, new crystals of AGA, which would allow us to collect higher resolution data, could not be grown and the source of AGA protein samples was no longer available. Thus, for several years AGA88 remained the only model of this enzyme.

Fig. 1. The AGA tetramer. Each subunit of the 222 symmetric molecule is colored differently. The spheres indicate active-site locations.

Nevertheless, AGA88 turned out to be invaluable for the solution of the structure of the first fully refined amidohydrolase, EcA. The crystallographic tetramer of AGA88 was used to locate the EcA tetramer in the asymmetric unit of its $P2_1$ unit cell by molecular replacement (MR), but was not sufficiently correct to allow for electron-density map interpretation or structure refinement. However, the MR phases revealed the heavy-atom sites of the only EcA heavy-atom derivative obtained (uranyl), which eventually became the primary source of EcA phases. Ultimately, the structural model of EcA was refined to an *R* factor of 0.145 at 2.3 Å resolution (Swain *et al.*, 1993) and has been used as the MR model to revise the structure of AGA, as described below.

Structure determination procedures leading to AGA88

Experimental methods for the growth of orthorhombic AGA crystals and for X-ray data collection have been described by Ammon *et al.* (1988). The space group is *I*222 with unit-cell parameters $a = 96.6$, $b = 112.5$, $c = 71.2$ Å. The X-ray diffraction data set, collected on a Picker FACS-I diffractometer, consisted of 9413 reflections, 7403 of which were observed [$F > 3\sigma(F)$]. The heavy-atom derivative data were collected in a similar manner, and the results obtained from difference Patterson maps are summarized in Table 1. Phases were refined with the programs *DICK* (Dickerson, Weinzierl & Palmer, 1968) and *PROTEIN* (Steigemann, 1974). Electron-density maps were calculated with multiple isomorphous replacement (MIR) phases to 4.7 Å resolution and single isomorphous replacement (SIR)

phases between 4.7 and 4.0 Å resolution. Density-modification techniques were used to enhance the maps and to extend the phases (Wang, 1985; Harrison, 1988). The resulting maps, and to a lesser extent the MIR/SIR map, were used to fit the preliminary model of AGA (AGA88).

Redetermination of the structure

Although the overall shape of the molecule and most of the secondary-structure elements were identified in AGA88, this model remained preliminary because of numerous errors in the linkages among these elements and/or improper chain direction. The current model of AGA (AGA94) (Fig. 2) is based on AGA88 and the refined structure of EcA (Swain *et al.*, 1993). The correct orientation of the AGA molecule in its unit cell was known from previous investigations (Ammon *et al.*, 1988). The starting model used in the current investigations was prepared as follows. The C_α representation of one EcA subunit was manually superimposed on the AGA88 subunit located in the AGA unit cell with the program *FRODO* (Jones, 1985). The fit was improved using the *FRODO* option RIGID for 84 C_α pairs, and the entire model (including side chains) of the EcA subunit was superimposed. This model was

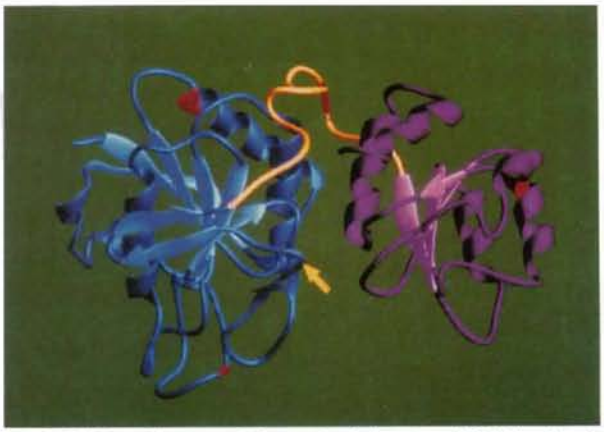

Fig. 2. Ribbon diagram of the main chain of an AGA94 subunit. The N-terminal domain is shown in blue with the eight-stranded β-sheet in the lighter shade; the C-terminal domain is purple with the β-sheet in the lighter shade; the interdomain linker is shown in yellow. Red indicates residues that are inserted in AGA relative to EcA (see Fig. 3). The yellow arrow indicates the sole deletion in AGA relative to EcA.

Table 2. *Refinement statistics of AGA94*

Resolution (Å)	10.0–2.9	
No. of reflections	7403	
No. of atoms	2497	
R factor*	0.171	
Weights†	$w = \sigma_F^{-2}$	
where	$\sigma_F = 50 - 50\ (\sin\theta/\lambda - 1/6)$	
R.m.s. deviations from ideality‡		
Distance restraints (Å)		
Bond distance	0.020	(0.020)
Angle distance	0.050	(0.030)
Planar 1–4 distance	0.065	(0.050)
Plane restraints (Å)	0.019	(0.020)
Chiral volume restraints (Å^3)	0.218	(0.150)
Non-bonded restraints (Å)		
Single-torsion contact	0.205	(0.500)
Multiple-torsion contact	0.253	(0.500)
Possible ($X\cdots Y$) hydrogen bond	0.201	(0.500)
Conformational torsion angles (°)		
Planar	4.3	(7.5)
Staggered	21.3	(10.0)
Orthonormal	29.8	(10.0)

* $R = \Sigma(|F_o - F_c|)/\Sigma(F_o)$.

† These are the standard weights recommended for *PROFFT* refinement.

‡ Target restraints are given in parentheses.

Fig. 3. Sequence alignment of AGA with EcA. EcA numbering is shown above (in blue), AGA numbering below (in red). Identical residues are shown in red, conserved residues in green.

adjusted to the $2F_o - F_c$ electron-density map that had been phased using the coordinates of AGA88.

The model was refined with *PROFFT* (Hendrickson, 1985; Finzel, 1987), using all observed X-ray data, to an R factor of 0.34. The first stage of model rebuilding was followed by refinement with *X-PLOR* (Brünger, Krukowski & Erickson, 1990), using a simulated-annealing strategy that lowered the R factor to 0.24 and yielded interpretable electron-density maps. Next, over numerous cycles, the amino-acid sequence of the model was changed to the correct sequence of AGA (Tanaka *et al.*, 1988) (the EcA subunit consists of 326 residues compared to 331 residues for AGA, Fig. 3). Because of the flexibility of some fragments of the AGA molecule *i.e.* the region between residues 10 and 35, the electron-density maps were not sufficiently clear to determine precisely their conformations. To decrease the model bias, we calculated several omit maps following grouped temperature-factor refinement (one B-factor value for main-chain atoms and one for side-chain and carbonyl O atoms per residue) with *X-PLOR*. Using *PROFFT*, we refined the final model (AGA94), which is comprised of 331 protein residues but no solvent, to an R factor of 0.171 for all X-ray intensity data with $F > 3\sigma(F)$ between 2.9 and 10.0 Å resolution. The weighting scheme used is that recommended in the *PROFFT* manual. Weights were applied to the data to give only very slightly higher weight to the higher resolution reflections. A summary of the final refinement statistics is given in Table 2.*

Comparison of AGA94 with AGA88

Although both models were created on the basis of the same X-ray intensity data, the limited extent of phasing and lack of information from models of other asparaginase structures prevented significant improvement of AGA88. AGA88 featured the correct overall shape and many of the secondary-structure elements of the molecule (Fig. 3 in Ammon *et al.*, 1988); however, one subunit consisted of two polypeptide chains comprised of 331 residues, arranged in two domains. None of the four loose ends of AGA88 correlate with the N or C termini of AGA94. Three of the ends are located near the ends of secondary-structure elements, where the density had not been clear enough to continue the trace. The remaining terminus ends a stretch of sequence that was built into density that actually belongs to the N-terminal domain of a symmetry-related subunit.

In AGA88, there are two crossovers between domains within the subunit, in contrast to the single linker indentified in AGA94 (Fig. 2). One of the connections in AGA88 follows the path of the linking strand in AGA94 and the other one is perpendicular to it. There is also a loop from the C-terminal domain of AGA88 that follows the interdomain linker of AGA94 and subsequently turns back into the C-terminal domain.

Thirteen secondary-structure elements were identified in AGA88 from the modified electron-density maps (Wang, 1985; Harrison, 1988), whereas 24 α-helices and β-strands are recognized in AGA94 (Fig. 4). Partly because of incorrect connections between the secondary-structure elements of AGA88, most of these have been traced in the opposite direction when compared with AGA94. Although the topology of some of the secondary-structure elements was described correctly in AGA88, distribution of these elements along the linear amino-acid chain is also much different from AGA94 because of errors in connectivities. Of 331 residues, 70 were modeled correctly; 121 were modeled in the correct topology, but in the wrong direction and 140 residues had no correspondence with the correct model.

A comparison of the main-chain torsion angles between AGA88 and AGA94 is illustrated with Ramachandran plots (Ramakrishnan & Ramachandran, 1965) in Fig. 5. In the case of AGA88, the (φ,ψ) values are scattered, whereas for AGA94 only two non-glycine residues (Thr200 and His300) are located far from the allowed regions of the Rama-

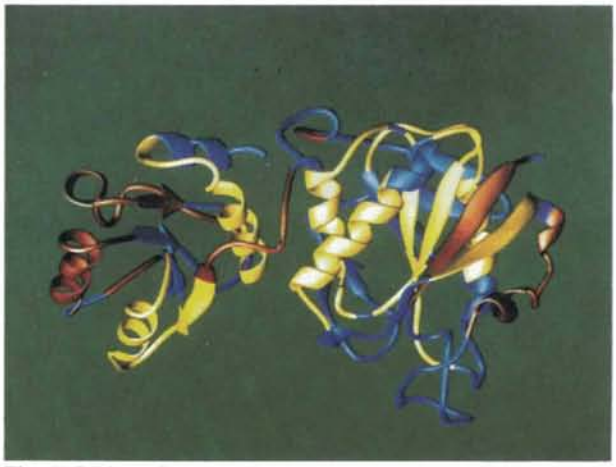

Fig. 4. Ribbon diagram of a subunit of AGA94, illustrating the agreement with AGA88. Brown represents fragments of AGA94 that match the topology and directionality of AGA88; yellow represents fragments of AGA94 for which the topology in AGA88 was identified correctly but the directionality was incorrect; blue represents regions that lack any topological relationship between AGA94 and AGA88.

* Atomic coordinates and structure factors have been deposited with the Protein Data Bank, Brookhaven National Laboratory (Reference: 1AGX, R1AGXSF). Free copies may be obtained through The Managing Editor, International Union of Crystallography, 5 Abbey Square, Chester CH1 2HU, England. (Reference: GR0331).

chandran plot. Both residues, however, are well defined in the electron density and their atypical conformations are stabilized by hydrogen bonds. One of the residues, Thr200, has nearly identical conformations in the models of EcA and ErA, and appears to stabilize the interdomain linker.

It is clear that the quality of AGA88 was limited by the poor quality of the electron-density maps that

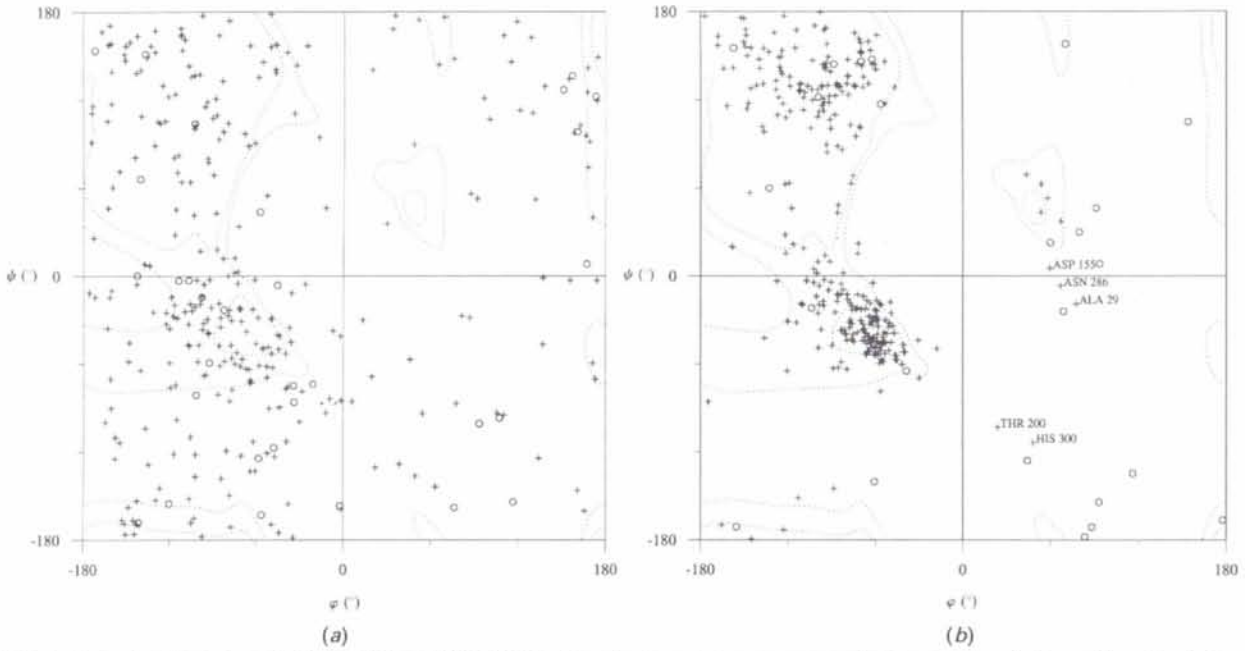

Fig. 5. Ramachandran plots of (*a*) AGA88 and (*b*) AGA94. Non-glycine residues are represented by crosses, glycine residues by circles. Residues located significantly outside of the allowed regions in AGA94 are labeled.

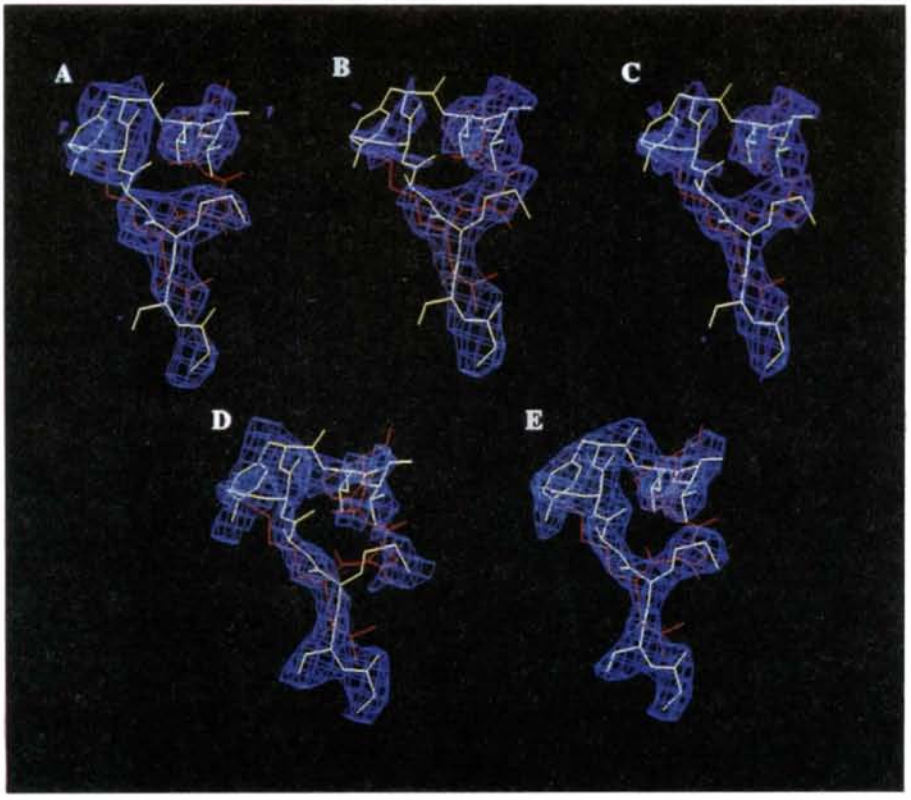

Fig. 6. A fragment of AGA88 (red) and AGA 94 (yellow) with electron-density maps superimposed. (*A*) MIR map calculated with the phases based on the heavy-atom positions listed in Table 1. (*B*) Map calculated with solvent-flattened and extended phases by the method of Wang (1985). (*C*) Map calculated with phases improved by histogram matching (Harrison, 1988). (*D*) $2F_o - F_c$ map calculated using phases from EcA superimposed on AGA. (*E*) $2F_o - F_c$ map calculated using phases from AGA94.

were strongly dependent on the initial phases obtained using MIR. To better understand the reasons why the initial MIR electron-density maps were so limited, we calculated the $F_{(derivative)} - F_{(native)}$ maps using AGA94 phases. We also repeated these calculations using AGA88 phases.* With respect to both the occupancies and positions of the heavy atoms, the results using phases obtained from AGA88 and AGA94 are similar (Table 1). This similarity suggests that no major errors were introduced in determining the heavy-atom parameters. Therefore, the phasing power of heavy-atom derivatives, even with phase extension, was insufficient to obtain more-readable electron-density maps.

The electron-density maps from which AGA88 had been built were visually compared, using computer graphics, with those obtained in the last stages of AGA94 building. This comparison was directed toward regions where significant errors either in connectivity or in protein-chain location were identified for AGA88. The electron-density maps from 1988 were consistent with the model, AGA88, showing no indication of chain polarity. Elsewhere, the maps were very sparse and unclear, not corresponding to either AGA88 or AGA94. These results support AGA88 as the best possible model that could be obtained from the data available at the time.

A fragment for which AGA88 and AGA94 are significantly different is presented in Fig. 6. In panels *A*, *B* and *C*, AGA88 superimposes best on the maps. Only the MR and final $2F_o - F_c$ maps (panels *D* and *E*) possess continuous density along the backbone of the correct model, AGA94. As observed previously (Ammon *et al.*, 1988), some of the density in the surface regions was removed by the use of automatically generated masks in the solvent-flattening procedure (panel *B*).

Comparison of AGA94 with EcA (the MR model)

The quaternary structures of AGA and EcA, including the spatial relationship between the domains, are the same, explaining the successful use of AGA88 as an MR probe for EcA. The r.m.s. deviation between C_α atoms of AGA94 and subunit 1 of EcA calculated with the program *ALIGN* (Satow, Cohen, Padlan & Davies, 1986) is 0.98 Å. Since the sequences of EcA and AGA are 42% identical, it is not surprising that their three-dimensional structures are very similar. AGA94 and EcA have essentially identical topologies with respect to secondary structure, though AGA is five residues longer. The first insertion in AGA relative to EcA is Ala24, a residue in the flexible loop that covers the active site (Figs. 2 and 3). The second insertion, Leu77 and Val78, occurs toward the C-terminal end of the second helix. However, structural compensation occurs by distending the loop after the helix in AGA relative to EcA. There is one deletion in AGA with respect to EcA, between residues 176 and 177, located in a loop involved in subunit contacts. The next insertion in AGA, Gln211 and Gly212, is in the linker region between the two domains, resulting in a loop that is absent in EcA. Finally, there is an insertion, Leu264, in the second helix of the C-terminal domain, which is compensated for by a lengthening of the preceding loop.

Active sites of amidohydrolases

Because of amino-acid sequence and topological similarity among all amidohydrolases studied crystallographically, it can be expected that the AGA active-site regions should superimpose very closely on those in EcA and ErA. Several of the residues forming the active site reside in flexible loops, some of which are located on the surface of the molecule. The AGA electron-density maps for part of this area have not been clear even in the final stages of refinement. The paucity of electron density in these areas is likely due to a combination of the flexibility of the enzyme in these regions and the limitation of the data. Water molecules have not been included in AGA94, although it is known that some of them play a significant role in creating the active-site constellations of EcA and ErA.

Taking these remarks into account, we can make a few general conclusions on the structure of the active-site region of AGA. Each active site consists of side chains belonging to two domains of adjacent subunits. From the structures of EcA and ErA and from the available enzymatic data (Bagert & Röhm, 1989; Wehner *et al.*, 1992; Derst, Hensling & Röhm, 1992), the following residues (with EcA numbering in parentheses) appear to be crucial for activity: Thr12(12), Tyr26(25), Ser59(58), Thr92(89), Asp93(90), Ser117(114), Lys165(162) in one subunit, and Ser252(248) and Glu288(283) from the adjacent subunit. These residues are similarly arranged in the structures of EcA, ErA and AGA. Several of the residues [Thr92(89), Asp93(90), Lys165(162) and Glu288(283) from the adjacent subunit] fit very well to the electron density with relatively low temperature factors. Two of the residues, Thr12(12) and especially Tyr26(25), have poorly defined electron densities and their conformations are not certain. Tyr26(25), located in the flexible loop, is positioned more deeply into the active site than its analog in EcA, forming an active site with a smaller volume. This result is unexpected, because AGA is capable of accommodating a larger substrate/product (glutamine/glutamate) in its active site. There is no indication

* We found that some of the heavy-atom coordinates reported previously (Table III, Ammon *et al.*, 1988) were mistyped.

from the crystallographic data of the presence of a ligand bound in the AGA active site, as in the cases of EcA and ErA, where aspartate or sulfate ligands are bound. Thus, it is not surprising that the active-site geometries may differ in detail.

Concluding remarks

The published model of *A. glutaminasificans* glutaminase–asparaginase, AGA88, was based on low-resolution data from native crystals, and even lower resolution data from heavy-atom derivative crystals. Because of the limitations of the data, AGA88 contained errors that prevented it from being a sufficient starting model in the solution of the structures of other asparaginases. Additional information was necessary to accurately phase the AGA data, but because it was not possible to collect more experimental information, we pursued the structures of closely related enzymes from different bacterial sources. The topological information obtained from the other asparaginases, along with the incorporation of the amino-acid sequence of AGA, produced better electron-density maps using the original X-ray diffraction data. This approach led to an improved and significantly different model, AGA94. The secondary-structure elements and their linkages have been verified, or redefined, resulting in a much better fit to the electron-density maps.

Although the active-site information from AGA94 is limited, a wealth of topological information has been gained, establishing the identical fold of asparaginases and glutaminase–asparaginases. This information will be used in a comparative study of the structures of amidohydrolases. The results presented here offer a good example of how a comprehensive study of a family of closely related proteins can provide information about every member of this family, even if the data for the individual members are not sufficient for this purpose.

We gratefully acknowledge the participation of Drs Lennart Sjölin and Robert Harrison in the early stages of this project and Anne Arthur for editorial assistance. This research was sponsored in part by the National Cancer Institute, DHHS under contract No. NO1-CO-74101 with ABL. The contents of this publication do not necessarily reflect the views or policies of the Department of Health and Human Services, nor does the mention of trade names, commercial products, or organizations imply endorsement by the US Government.

References

AMMON, H. L., MURPHY, K. C., SJÖLIN, L., WLODAWER, A., HOLCENBERG, J. S. & ROBERTS, J. (1983). *Acta Cryst.* **B39**, 250–257.

AMMON, H. L., WEBER, I. T., WLODAWER, A., HARRISON, R. W., GILLILAND, G. L., MURPHY, K. C., SJÖLIN, L. & ROBERTS, J. (1988). *J. Biol. Chem.* **263**, 150–156.

BAGERT, U. & RÖHM, K. H. (1989). *Biochim. Biophys. Acta*, **999**, 36–41.

BRÜNGER, A. T., KRUKOWSKI, A. & ERICKSON, J. (1990). *Acta Cryst.* **A46**, 585–593.

DERST, C., HENSELING, J. & RÖHM, K. H. (1992). *Protein Eng.* **5**, 785–789.

DICKERSON, R. E., WEINZIERL, J. E. & PALMER, R. A. (1968). *Acta Cryst.* **B24**, 997–1003.

EPP, O., STEIGEMANN, W., FORMANEK, H. & HUBER, R. (1971). *Eur. J. Biochem.* **20**, 432–437.

FINZEL, B. C. (1987). *J. Appl. Cryst.* **20**, 53–55.

HARRISON, R. W. (1988). *J. Appl. Cryst.* **21**, 949–952.

HENDRICKSON, W. A. (1985). *Methods Enzymol.* **115**, 252–270.

HOLCENBERG, J. S. & ROBERTS, J. (1977). *Annu. Rev. Pharmacol. Toxicol.* **17**, 97–116.

JONES, A. T. (1985). *Methods Enzymol.* **115**, 157–171.

MILLER, M., RAO, J. K. M., WLODAWER, A. & GRIBSKOV, M. R. (1993). *FEBS Lett.* **328**(3), 275–279.

RAMAKRISHNAN, C. & RAMACHANDRAN, G. N. (1965). *Biophys. J.* **5**, 909–933.

ROBERTS, J., HOLCENBERG, J. S. & DOLOWY, W. C. (1970). *Nature (London)*, **227**, 1136.

ROBERTS, J., HOLCENBERG, J. S. & DOLOWY, W. C. (1972). *J. Biol. Chem.* **247**, 84–90.

ROBERTS, J., SCHMID, F. A., OLD, L. J. & STOCKERT, E. (1976). *Cancer Biochem. Biophys.* **1**, 175–178.

SATOW, Y., COHEN, G. H., PADLAN, E. A. & DAVIES, D. A. (1986). *J. Mol. Biol.* **190**, 593–604.

STEIGEMANN, W. (1974). PhD thesis, Technische Univ. München, Germany.

SWAIN, A. L., JASKÓLSKI, M., HOUSSET, D., RAO, J. K. M. & WLODAWER, A. (1993). *Proc. Natl. Acad. Sci. USA*, **90**, 1474–1478.

TANAKA, S., ROBINSON, E. A., APPELLA, E., MILLER, M., AMMON, H. L., WEBER, I. T. & WLODAWER, A. (1988). *J. Biol. Chem.* **263**, 8583–8591.

WADE, H. E. (1980). *Microorganisms and Nitrogen Sources*, edited by J. W. PAYNE, pp. 563–575. New York: John Wiley.

WANG, B.-C. (1985). *Methods Enzymol.* **115**, 90–112.

WEHNER, A., HARMS, E., JENNINGS, M. P., BEACHAM, I. R., DERST, C., BAST, P. & RÖHM, K. H. (1992). *Eur. J. Biochem.* **208**, 475–480.

WLODAWER, A., ROBERTS, J. & HOLCENBERG, J. S. (1977). *J. Mol. Biol.* **112**, 515–519.